**Smart Structures and Systems**, *Vol. 27, No. 5 (2021) 769-781*
DOI: https://doi.org/10.12989/sss.2021.27.5.769


# Design and analysis of plate-type eddy-current damper with high energy-dissipation capability

Jiazeng Shan [1a], Jie Liu [1b], Cheng Ning Loong[*2] and Weichao Wu [1c]

[1] *Department of Disaster Mitigation for Structures, Tongji University, Shanghai 200092, China*
[2] *Department of Civil and Environmental Engineering, The Hong Kong University of Science and Technology, Kowloon, Hong Kong, China*

(*Received May 23, 2020, Revised October 14, 2020, Accepted January 6, 2021*)

**Abstract.** A plate-type eddy-current damper with high energy-dissipation capability is designed and analyzed. The damper is configured in a dimension of 270 mm × 500 mm × 80 mm by employing 16 pairs of rectangular magnets and a rectangular copper plate. The paired magnets are arranged as two rows of 4-by-4 arrays with polarities alternating along the moving direction, while the copper plate is embedded inside two rows of magnets. A finite-element model is developed to investigate eddy-current force. The damping coefficient of damper under a constant velocity of 0.2 m/s is 24.44 kN-s/m. The eddy-current force under harmonic motion can be fitted as a sum of a linear elastic force and a linear damping force. The stiffness coefficient is increased by 77 times and the damping coefficient is reduced relatively by 19%, for vibration frequency increased from 0.5 to 10.0 Hz. The sensitivity of stiffness and damping coefficients on the physical dimensions of magnet and copper plate are discussed. The phase lag is sensitive to copper-plate thickness but insensitive to clear gap between two rows of magnets. The damper is implemented on a based-isolated structure. It is shown that the damper could reduce the peak of base drift and absolute acceleration response spectra by 71.9% and 73.1%, respectively.

**Keywords:** Eddy-current damping; hysteretic nonlinearity; frequency dependence; energy dissipation; finite element modeling

## 1. Introduction

The eddy-current damper is a control device operating based on the generation of an eddy current. One possible physical mechanism generating the eddy current is via a relative movement between a conductor and a permanent magnet. Through this mechanism, the conductor is subjected to a time-varying magnetic field, and an eddy-current force is simultaneously produced to oppose the relative movement (Zuo *et al*. 2011). Due to this non-contact characteristic, the eddy-current damper is less likely to be damaged during operation. The eddy-current damper is also relatively reliable regarding the temperature variations (Wang *et al*. 2017). It is indicated that the eddy-current damper could have a longer service life than some dampers, such as the viscous damper and the friction damper, which could suffer from the leakage problem and wearing damage, respectively (Wang *et al*. 2012).

With these desired advantages, the eddy-current damper has been studied for vibration mitigation of automobiles, precision instrumentations, civil engineering structures, etc. (Bae *et al*. 2014, Diez-Jimenez *et al*. 2019). Sodano *et al*. (2005) investigated the performance of an eddy-current damper in reducing the vibration of a cantilever beam. Experimental results showed that the tip displacement of the beam was suppressed by 42.4 dB at its first modal frequency. Chen *et al*. (2013) designed an eddy-current damper to reduce the vibration of a force sensor. Results showed that the damper could suppress the sensor vibration under an impact excitation by about 30 dB. Eddy-current damper could also be equipped to a tuned mass damper to reduce the vibration of a large-scale structure. Feudo *et al*. (2017) showed that an eddy-current damper attaching on a tuned mass damper could reduce structural vibration at the first resonance by more than 80%. Results from Lu *et al*. (2017) showed that the eddy-current damper equipped to a tuned mass damper could reduce the wind-induced acceleration and the earthquake-induced displacement of a high-rise building by about 45 to 60% and 5 to 15%, respectively. With these promising results, an eddy-current damper has been implemented with the tuned mass damper in the Shanghai Center Tower, and satisfactory control performance was observed in the field monitoring data obtained from a typhoon event (Lu *et al*. 2019).

Eddy-current damper with a sufficiently large damping coefficient is needed for vibration mitigation. This damping coefficient is affected by the materials used for manufacturing the damper and their topological configurations (Ebrahimi *et al*. 2008, Ao and Reynolds 2019). Ebrahimi *et al*. (2009) designed a cylindrical eddy-current damper with radially magnetized magnets. The magnets were arranged with the Halbach array pattern, i.e., each magnet was arranged with the magnetic pole being

*Corresponding author, Postdoctoral Fellow,
E-mail: cnloong@connect.ust.hk
[a] Associate Professor, E-mail: jzshan@tongji.edu.cn
[b] Graduate Student, E-mail: 1832279@tongji.edu.cn
[c] Graduate Student, E-mail: wuweichao@tongji.edu.cn



ISSN: 1738-1584 (Print), 1738-1991 (Online)

rotated by 90 degrees to its adjacent magnets. Results showed that the prototyped damper could provide a damping coefficient of up to 1.8 kN-s/m. Zuo *et al*. (2011) designed an eddy-current damper with four copper plates embedding inside five layers of magnet components. The magnets in each layer were arranged with an alternating polarity. Results showed that the designed damper with a size of 100 mm × 153 mm × 140 mm could provide a damping coefficient up to 2.2 kN-s/m. Huang *et al*. (2018) developed an eddy-current damper with soft irons embedding outside of the magnets of the damper. They showed that the damping coefficient of the damper could be increased from 61 to 321 Ns/m by the inclusion of soft irons. Li *et al*. (2019) enhanced the damping capability of an eddy-current damper by adopting a ball screw and a gearbox for linear-to-rotational motion conversion. It was reported that the damper with a volume of $1.10 \times 10^6$ mm$^3$ could provide a damping coefficient up to 1155 kN-s/m.

In some studies, the eddy-current force is assumed linearly to the relative velocity between magnet and conductor (Wang *et al*. 2012). This linear force-velocity assumption might be valid for low-velocity magnitude (Huang *et al*. 2018). Under a large or time-varying velocity, the eddy-current force becomes nonlinear and hysteretic to the velocity. These phenomena have been observed and reported by some researchers such as Ebrahimi *et al*. (2008), Zuo *et al*. (2011), etc. Under a harmonic motion, the eddy-current force is found providing both linear damping force and linear elastic force. The stiffness coefficient of the elastic force and the damping coefficient of the damping force respectively increases and decreases with vibration frequency (Loong *et al*. 2020). Bae *et al*. (2009) reported that the stiffness coefficient and damping coefficient of the eddy-current force were respectively increased by about 9.9 times and reduced by about 60% for vibration frequency increased from 1 to 8 Hz. Pan *et al*. (2016) also showed that the damping coefficient was reduced by 51% when the vibration frequency changed from 1 to 10 Hz. This vibration-dependent behavior of the eddy-current force would affect the vibration mitigation performance of the damper. For instance, the authors of the present study illustrated that neglecting the reduction of damping coefficient in the analysis could underestimate the total acceleration and relative displacement of a structure equipped with an eddy-current damper under ground excitations (Loong *et al*. 2020). It indicates that the nonlinearity of the eddy-current force is apparently an important issue that should be addressed.

In this study, a plate-type eddy-current damper with a high-energy dissipation capability is designed and analyzed. The proposed eddy-current damper can provide a two-dimensional planer damping force. As shown in the later sections, under a given volume, the proposed damper could provide a relatively large damping coefficient than that of some eddy-current dampers presented in the literature. A finite-element model is developed in ANSYS (2018) to investigate the eddy-current force generated by the damper. The hysteretic nonlinearity presented in the eddy-current force under a harmonic motion is examined. The effects of design parameters on the hysteretic nonlinearity in the eddy-current force are further discussed. The damper is then implemented on a base-isolated structure to illustrate its feasibility for vibration mitigation.

## 2. Design of the Plate-type Eddy-current Damper

Fig. 1 shows the notation for describing an eddy-current damper made by two pairs of rectangular magnets and a rectangular conductor plate. All magnets have identical dimensions with width × length × thickness, denoted as $w_m \times l_m \times t_m$. The north (N) and the south (S) poles of magnets are expressed as a cross and a filled circle, respectively. Magnets in the same column have the same polarity direction (see Fig. 1(b)). The clearance $d$ and the clear gap $g$ are defined as the distance between two adjacent magnets at the same layer and the distance between two magnets in the same column, respectively. The conductor is made by a copper plate with a dimension of $w_c \times l_c \times t_c$. This conductor embedding inside the middle of the magnet layer is moving with a relative displacement $u$. An eddy-current force $F$ is simultaneously generated to

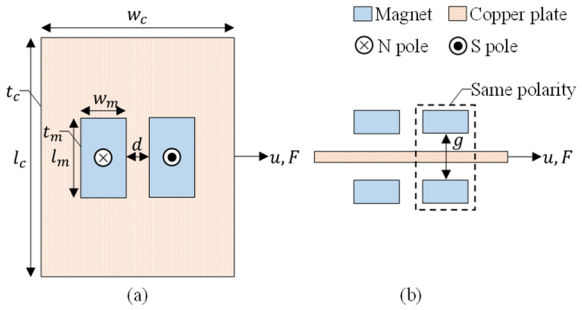


Fig. 1 Notation for modeling of eddy-current damper made by rectangular permanent magnets and rectangular conductor plate: (a) plan view; (b) elevation view

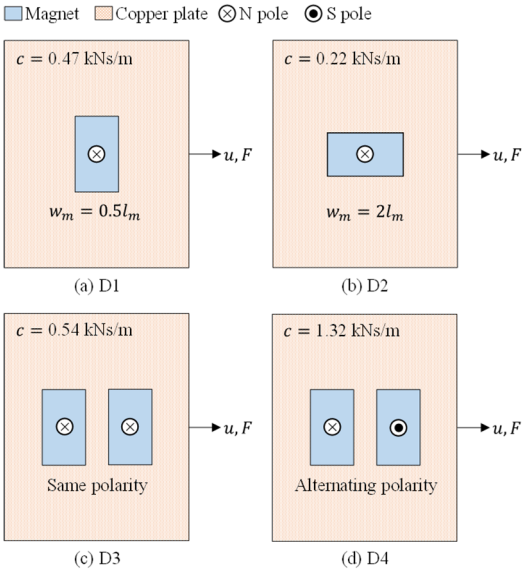


Fig. 2 Illustrative examples of four different eddy-current damper designs: (a) D1; (b) D2; (c) D3; (d) D4

oppose this relative movement. In this study, analysis is conducted in ANSYS (2018) with a time step of $2\times10^{-3}$ s.

Preliminary analysis is performed to demonstrate the design idea of a plate-type eddy-current damper with a high energy-dissipation capability. Fig. 2 shows four eddy-current damper designs, which are denoted as D1, D2, D3, and D4, respectively. The copper plate having dimensions of $w_c \times l_c \times t_c$ = 270 mm × 490 mm × 6 mm, is allocated in the middle of magnets with $g$ = 10 mm. The conductivity of the copper plate is assumed as $5.8\times10^7$ S/m (Huang *et al*. 2018). The dimensions of magnets for D1, D3, and D4 are $w_m \times l_m \times t_m$ = 50 mm × 100 mm × 25 mm while that for D2 is 100 mm × 50 mm × 25 mm. The magnets are made by NdFeB grade N35 with a remanent flux density of 1.45 T and relative permeability of 1. Both the copper plate and the paired magnets are modeled with mesh sizes of 20 mm. It can be seen that D1 and D2 have identical magnets, but the orientation of magnets for D2 is 90º rotated. D3 and D4 are made by two pairs of magnets with $d$ = 10 mm. The polarity direction for D3 is the same, while that for D4 is alternating along with the direction of motion.

To quantify the damping capability of a damper design, damping coefficient of the damper is adopted. The damping coefficient $c$ is defined as the ratio of eddy-current force $F$ over the constant relative velocity at stationary $\dot{u}$ as

$$c \equiv \frac{F}{\dot{u}} \tag{1}$$

Fig. 2 shows that the damping coefficient $c$ of D1, D2, D3 and D4 under a constant relative velocity $\dot{u} = 0.2$ m/s are 0.47, 0.22, 0.54 and 1.32 kN-s/m, respectively. The damping coefficient for D1 is two times more than that for D2. It indicates that the longer side of the magnet should be aligned perpendicularly to the moving direction. This is because the eddy-current force is positively related to the rate of changes in magnetic flux. Under an increment of time and a constant velocity, the changes of magnetic flux are related to the area formed by the length of the magnet and the moving distance. Since the length of D1 is larger than that of D2, the changes of magnetic flux for D1 will be larger than that for D2, which leads to a larger eddy-current force. Generally, under a given area of magnet, the magnet length should be sufficiently large to generate a large eddy-current force (Heald 1988). However, there exists an optimal $w_m/l_m$ to minimize the damper cost. As shown in Schieber (1975), the optimal $w_m/l_m$ should be ranging from 0.3 to 0.5. Hence, $w_m/l_m = 0.5$ is adopted hereinafter in this study.

Figs. 2(c)-(d) respectively show that the damping coefficients for D4 and D3 are 2.81 and 1.15 times of that for D1. As expected, increasing the number of magnets enhances the damping coefficients. Results show that the alternating polarity configuration along the direction of motion, such as the design of D4, could enhance the damping coefficient, as compared to that with the same polarity configuration. It indicates that the alternating polarity is an efficient approach to increase the damping coefficient. To explain, the instantaneous eddy-current density $J$ for D3 and D4 of the middle of the copper plate at simulation time equals to 0.1 s are shown in Fig. 3. It can be seen that D4 has a larger magnitude of eddy-current density than that of D3. An additional eddy-current loop is observed in between two adjacent magnets with alternating

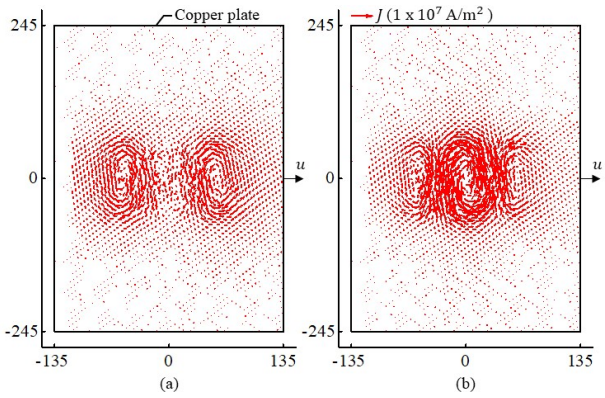


Fig. 3 Comparison of eddy-current density $J$ at the middle of copper plate between (a) D3; and (b) D4

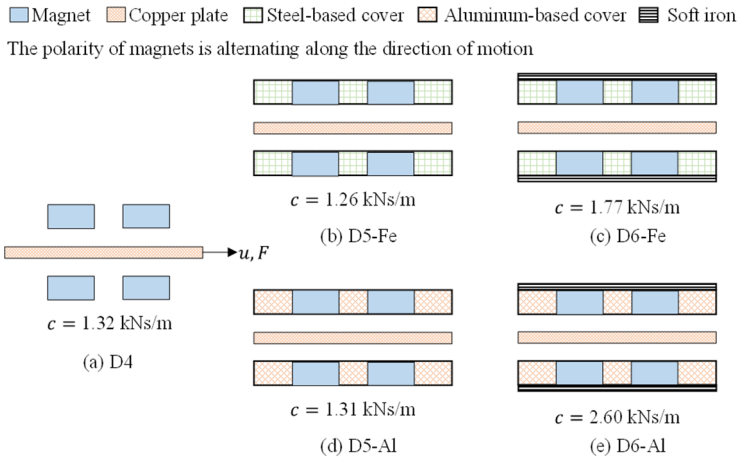


Fig. 4 Comparison between eddy-current damper designs with and without cover or soft iron: (a) D4; (b) D5-Fe; (c) D6-Fe; (d) D5-Al and (e) D6-Al

polarities. It indicates that the current density is intensified by the design of D4, which is beneficial for improving the damping capability of the eddy-current damper. This analysis is consistent with the results shown in Zuo *et al.* (2011) and Wang *et al*. (2012).

D4 is further incorporated with steel-based cover (D5-Fe) and soft irons (D6-Fe) or aluminum-based cover (D5-Al) and soft irons (D6-Al), as shown in Fig. 4. The dimensions of soft irons are 250 mm × 480 mm × 10 mm, while that of the steel-based or the aluminum-based cover, with magnets embedded, are 250 mm × 480 mm × 25 mm. The conductivity of the soft iron, steel, and aluminum are set as $1.0 \times 10^7$, $2.0 \times 10^6$, and $3.8 \times 10^7$ S/m, respectively. The relative permeability of soft iron and aluminum are set as 4000 and 1.0, respectively (Engineering ToolBox 2001), while that of the steel is set

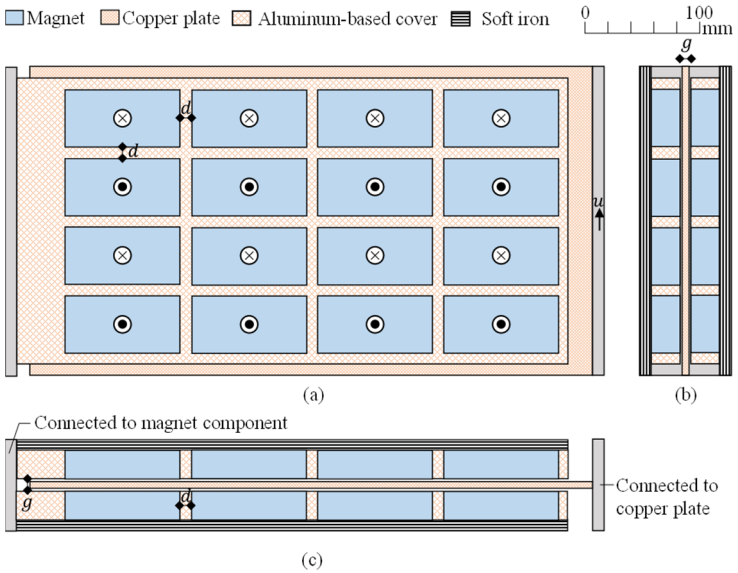


Fig. 5 Schematic drawing of the proposed plate-type eddy-current damper with high energy-dissipation: (a) elevation view; (b) plan view; (c) cross-sectional view

Table 1 Parameters for finite-element modeling of the proposed plate-type eddy-current damper in ANSYS

| Descriptions | Properties | Value |
|---|---|---|
| Magnet | $w_m \times l_m \times t_m$ | 50 mm × 100 mm × 25 mm |
| | NdFeB | Grade N35 |
| | $d$ | 10 mm |
| | $g$ | 10 mm |
| | Number | 16 pairs |
| | Remanent flux density | 1.45 T |
| | Relative permeability | 1 |
| Copper plate | $w_c \times l_c \times t_c$ | 270 mm × 490 mm × 6 mm |
| | Number | 1 |
| | Conductivity | $5.8 \times 10^7$ S/m |
| | Relative permeability | 1 |
| Aluminum-based cover | $w_a \times l_a \times t_a$ (including magnets) | 250 mm × 480 mm × 25 mm |
| | Number | 1 pair |
| | Conductivity | $3.8 \times 10^7$ S/m |
| | Relative permeability | 1 |
| Soft iron | $w_s \times l_s \times t_s$ | 250 mm × 480 mm × 10 mm |
| | Number | 1 pair |
| | Conductivity | $1.0 \times 10^7$ S/m |
| | Relative permeability | 4000 |

based on the magnetic-flux-density-field-strength curve (*B-H* curve) developed based on the Steel 1008, which is available in ANSYS (2018). The damping coefficients for D5-Fe and D6-Fe are 1.26 and 1.77 kN-s/m, which are about 0.95 and 1.34 times of D4, respectively. The damping coefficients for D5-Al and D6-Al are 1.31 and 2.60 kN-s/m, which are about 0.99 and 1.97 times of D4, respectively. It is seen that the inclusion of steel-based cover has a negligible adverse effect on the damping coefficient. Results also indicate that adopting aluminum is better than steel as the cover. The soft irons embedded outside the magnets increase the damping capability of damper (Huang *et al*. 2018). The combinations of aluminum-based cover and soft irons (D6-Al) increase the damping coefficient of D4 by almost 2 times.

The aforementioned analysis has inspired the design of the proposed plate-type eddy-current damper, as shown in Fig. 5. Table 1 shows the details of the design parameters for the proposed damper. The proposed damper is composed of a magnet component and a copper plate. The magnet component consists of 16 pairs of rectangular magnets, arranged with a 4-by-4 array. The sizes of each magnet and the copper plate are 50 mm × 100 mm × 25 mm and 270 mm × 490 mm × 6 mm, respectively. The polarity of a magnet is alternating along the direction of motion $u$. Each row of magnets is embedded inside an aluminum-base cover that is contained by a soft iron (see Figs. 5(b)-(c)). The copper plate sandwiching inside two rows of magnets are allowed to move perpendicular to the longer side of magnets. The clearance $d$ and the clear gap $g$ are both set as 10 mm. Fig. 6 shows the finite element modeling of the proposed damper using ANSYS (2018). The copper plate, magnets, aluminum-based cover, and soft iron are modeled with mesh sizes of 10, 20, 30, and 30 mm, respectively. These mesh sizes are chosen to simulate the eddy-current force with sufficient accuracy while ensuring that the computational efforts for the numerical simulations are manageable by a computer with two 10-core CPUs and 128 GB memory.

Including the size of soft irons, the size of aluminum-based covers, and the clear gap between magnets, the volume of the proposed eddy-current damper is 270 mm × 500 mm × 80 mm. Finite element analysis shows that the proposed eddy-current damper provides a damping coefficient of 24.44 kN-s/m under a constant velocity of 0.2 m/s. It indicates that the damping density of the proposed eddy-current damper, which is defined as the ratio of damping coefficient over the volume of damper, is 2.26 MNs/m/m$^3$. This damping density is two times higher than that of the plate-type eddy-current damper developed by Zuo *et al*. (2011) with a value of 1.06 MNs/m/m$^3$. The reasons attributed to a higher damping density of the proposed damper include: (1) the proposed damper adopts the aluminum-based cover; (2) the number of magnets per unit volume of the proposed eddy-current damper is higher than that developed by Zuo *et al*. (2011). The proposed eddy-current damper could be applied for vibration control that needs a planner-movement damping mechanism. For instance, it could be equipped to a tuned mass damper for mitigating the vibration of a high-rise building. It could be

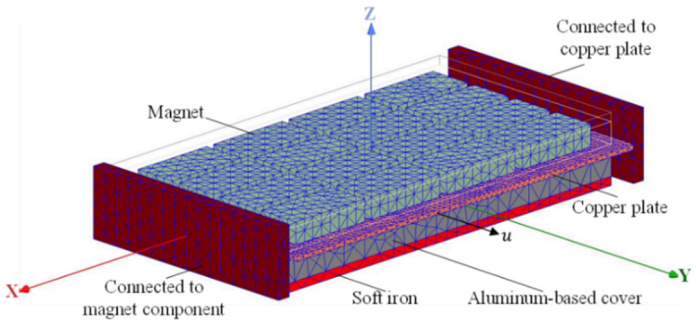


Fig. 6 Finite element modeling of the proposed eddy-current damper using ANSYS

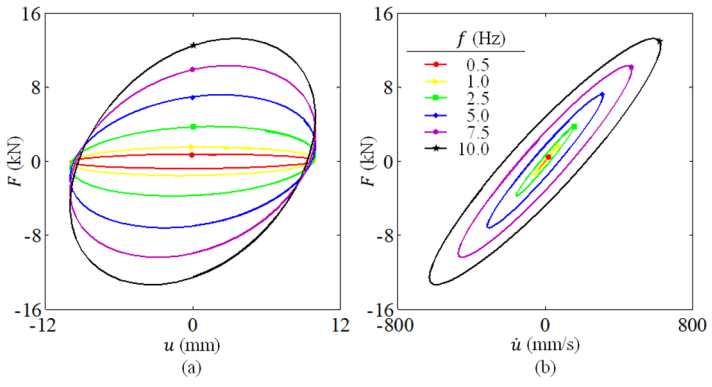


Fig. 7 Eddy-current force $F$ under harmonic motion with a vibration amplitude $A$ = 10 mm and a vibration frequency $f$ = 0.5, 1.0, 2.5, 5.0, 7.5 and 10.0 Hz: (a) force-displacement curve; and (b) force-velocity curve

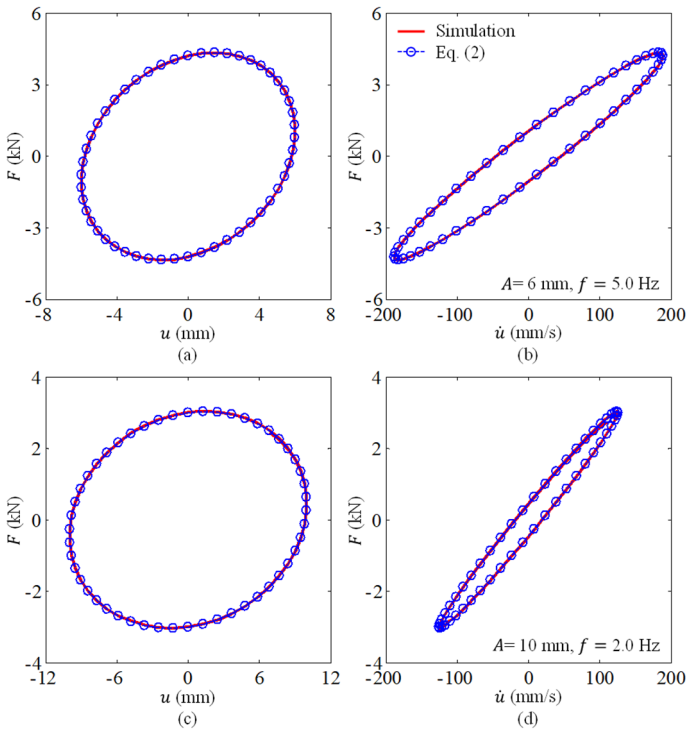


Fig. 8 Comparison of eddy-current force between the results generated from ANSYS and that reconstructed using Eq. (2): (a) force-displacement; and (b) force-velocity curves under $A$ = 6 mm, $f$ = 5.0 Hz; (c) force-displacement and (d) force-velocity curves under $A$ = 10 mm, $f$ = 2.0 Hz

used as a supplemental dissipative device for a base-isolated structure. It could also be adopted as the energy consumption element in a replaceable coupling beam, such as the one patented by Wu *et al.* (2018) and their colleagues.

## 3. Eddy-current force under harmonic motion

The eddy-current force generated from the proposed eddy-current damper under a harmonic motion with a vibration amplitude $A$ and a vibration frequency $f$ is examined. This study focuses on the vibration control of a civil engineering structure, which normally vibrates with a frequency of less than 10 Hz (Zhu *et al.* 2012). The vibration amplitude is assumed between 4 and 12 mm.

Figs. 7(a)-(b) respectively show the eddy-current force-displacement and force-velocity curves under vibration amplitude $A$ = 10 mm and vibration frequency $f$ = 0.5, 1.0, 2.5, 5.0, 7.5 and 10.0 Hz. Under a relatively low vibration frequency, e.g., $f$ = 0.5 and 1.0 Hz, the force-displacement curve is an ellipse without notable inclination and the force is linearly related to the velocity without a loop. It indicates that under low $f$, the proposed damper behaves practically as a linear viscous damper that can be characterized by a constant damping coefficient. Under a relatively high vibration frequency, e.g., $f$ = 7.5 and 10.0 Hz, the force-displacement curve becomes an inclined ellipse and the force-velocity curve consists of loops. The inclination for force-displacement curve increases with $f$, while the slope for the force-velocity curve slightly decreases with $f$. The eddy-current force is shown hysteretic under high vibration frequency. It indicates that a certain "stiffness" behavior exists in the eddy-current force.

To analyze, it is assumed that the eddy-current force $F$ can be fitted as the sum of a linear elastic force $k_{eq}u$ and a linear damping force $c_{eq}\dot{u}$ as

$$F = k_{eq}u + c_{eq}\dot{u} \tag{2}$$

where $k_{eq}$ and $c_{eq}$ are the equivalent stiffness coefficient and the equivalent damping coefficient of the linear elastic force and the linear damping force under harmonic motions, respectively. The values of $k_{eq}$ and $c_{eq}$ can be obtained by fitting the eddy-current force generated from the numerical simulation with Eq. (2) using the minimum mean-squared error criteria. Fig. 8 compares the eddy-current force $F$ simulated using ANSYS (2018) and the results reconstructed using Eq. (2), under $A$ = 6 mm, $f$ = 5.0 Hz as well as $A$ = 10 mm, $f$ = 2.0 Hz. Results show that Eq. (2) can fit the eddy-current force quite well. It indicates that Eq. (2) is sufficient to characterize the hysteretic nonlinearity presented in eddy-current force under a harmonic motion.

The details of the fitted equivalent stiffness coefficient $k_{eq}$ and the fitted equivalent damping coefficient $c_{eq}$ under different vibration frequency $f$ are summarized in Table 2. Fig. 9 shows the variation of $k_{eq}$ and $c_{eq}$ as a function of $f$, under vibration amplitude $A$ = 10 mm. It is shown that the stiffness coefficient $k_{eq}$ and the damping coefficient $c_{eq}$ increase and decrease with vibration frequency $f$, respectively. The value of $k_{eq}$ is increased from 6.09 to 471.92 kN/m, while the value of $c_{eq}$ is

Table 2 Variation of equivalent stiffness coefficient $k_{eq}$ and equivalent damping coefficient $c_{eq}$ with respect to vibration frequency $f$ under a vibration amplitude $A$ =10 mm

| Frequency $f$ (Hz) | Stiffness coefficient $k_{eq}$ (kN/m) | Damping coefficient $c_{eq}$ (kN-s/m) |
|---|---|---|
| 0.5 | 6.09 | 24.55 |
| 1.0 | 16.32 | 24.37 |
| 1.5 | 29.44 | 24.12 |
| 2.0 | 44.98 | 23.86 |
| 2.5 | 62.47 | 23.58 |
| 3.0 | 81.38 | 23.28 |
| 4.0 | 124.10 | 22.76 |
| 5.0 | 173.07 | 22.27 |
| 7.5 | 311.14 | 21.08 |
| 10.0 | 471.92 | 19.93 |

decreased from 24.55 to 19.93 kN-s/m, for $f$ increases from 0.5 to 10.0 Hz. The increase in $k_{eq}$ is about 77 times while the relative reduction of $c_{eq}$ is about 19%. The vibration-dependent behavior of $k_{eq}$ and $c_{eq}$ would affect the vibration control performance of the eddy-current damper. This issue is important particularly for applications that are sensitive to vibration characteristics. For instance, an eddy-current damper connecting to a tuned mass damper would require a proper tuning of frequency. Neglecting the vibration-dependent behavior presented in the eddy-current force during the design stage would lead to a non-optimal design. Next, the effects of vibration amplitude are studied. Fig. 10 shows the variation of $k_{eq}$ and $c_{eq}$ as a function of $A$, under $f$ = 5.0 Hz. Results show that the values of $k_{eq}$ and $c_{eq}$ are relatively insensitive to the vibration amplitude considered in the analysis. It seems that the nonlinearity of the eddy-current force is more sensitive to the vibration frequency than the vibration amplitude. Overall, it indicates that the nonlinearity of eddy-current force should be considered in the analysis especially for applications involving relatively high vibration frequency.

Next, the reasons for the increase of stiffness coefficient and the decrease of damping coefficients with respect to vibration frequency are discussed. Similar to skin effects (Kazimierczuk 2014), the hysteretic nonlinearity presented in the eddy-current force is affected by the time-varying eddy current induced on the copper plate (Bae *et al*. 2009, Zuo *et al*. 2011). This time-varying eddy current, which produced by the non-constant relative velocity motion, generates an additional time-varying magnetic field that reduces the magnetic field provided by the magnets. The overall magnetic field is reduced and leads to a reduction of the damping coefficient. It should be noted that this additional time-varying magnetic field is generally not in phase with the magnetic field provided by the magnets. This results in a phase difference between the eddy-current force and the relative velocity. To explain, suppose that the relative displacement and the relative velocity of the

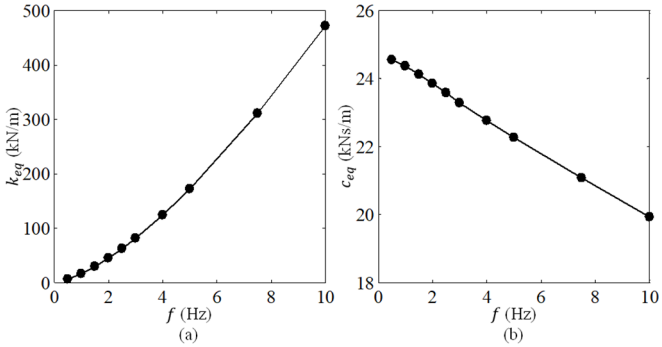


Fig. 9 Variation of (a) equivalent stiffness coefficient $k_{eq}$; and (b) equivalent damping coefficient $c_{eq}$ as a function of vibration frequency $f$, under vibration amplitude $A$ = 10 mm

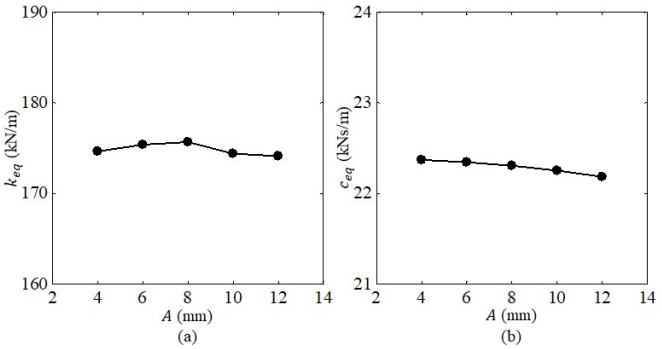


Fig. 10 Variation of (a) equivalent stiffness coefficient $k_{eq}$ and (b) equivalent damping coefficient $c_{eq}$ as a function of vibration amplitude $A$, under vibration frequency $f$= 5.0 Hz

harmonic motions are respectively denoted as $u = A\sin(2\pi ft)$ and $\dot{u} = 2\pi fA\cos(2\pi ft)$, the eddy-current force with a phase lag $\phi$ to the velocity can be expressed as

$$F = 2\pi fAc\cos(2\pi ft - \phi) \tag{3}$$

in which $c$ is defined in Eq. (1). After some algebraic manipulations, Eq. (3) can be rewritten as

$$F = k_{eq}u + c_{eq}\dot{u} \tag{4}$$

where the equivalent stiffness coefficient $k_{eq}$ and the equivalent damping coefficient $c_{eq}$ that can be found related to $c$, $f$, and $\phi$ as follows

$$k_{eq} = 2\pi fc\sin\phi \tag{5}$$

$$c_{eq} = c\cos\phi \tag{6}$$

Within the regime of low velocities under which Eq. (1) is valid, suppose that $c$ is insensitive to the variation of velocity magnitude and since the phase lag $\phi$ is positively related to the vibration frequency $f$ (Kazimierczuk 2014), Eqs. (5)-(6) show that $k_{eq}$ and $c_{eq}$ are functions that respectively increase and decrease with $f$. Eqs. (5)-(6) also show that $k_{eq}$ and $c_{eq}$ are insensitive to the vibration amplitude $A$. The results shown in Eqs. (4)-(6) are consistent with the results obtained from the previous analysis in this section, i.e., the eddy-current force behaves as a combination of a linear elastic force $k_{eq}u$ and a linear damping force $c_{eq}\dot{u}$, with equivalent stiffness coefficient $k_{eq}$ and equivalent damping coefficient $c_{eq}$ that respectively increase and decrease with vibration frequency $f$. It should be noted that although a sine function is assumed for relative displacement $u$, the analysis is applicable for cosine function, it is not shown in the study for brevity. It should be noted that the assumption for the insensitivity of $c$ to the variation of velocity magnitude is only valid under low velocity magnitude. The generation of eddy-current force, which modeled by Shi *et al*. (2020) using an equivalent circuit model made by a voltage source connecting in series with a resistor and an inductor, showed that the damping coefficient $c$ was a decreasing function of vibration frequency. In the regime of relative high velocities, Bourquin *et al*. (2014) adopted the Maxwell receding image method to show that the damping coefficient was a decreasing function of velocity magnitude. Huang *et al*. (2018) also simulated this phenomenon for their designed eddy-current damper and pointed out that the relationship between the eddy-current force and the relative velocity was linear only for velocity less than 1.0 m/s. Hence, the maximum damping force was found to increase with velocity, but the increasing rate decreased with the velocity magnitude (Ebrahimi *et al*. 2009, Huang *et al*. 2018). Summarizing the results shown in the previous and the present studies, the reduction of damping coefficient $c$ due to high velocity magnitude mainly affects the maximum damping force generated by the damper, while the phase lag

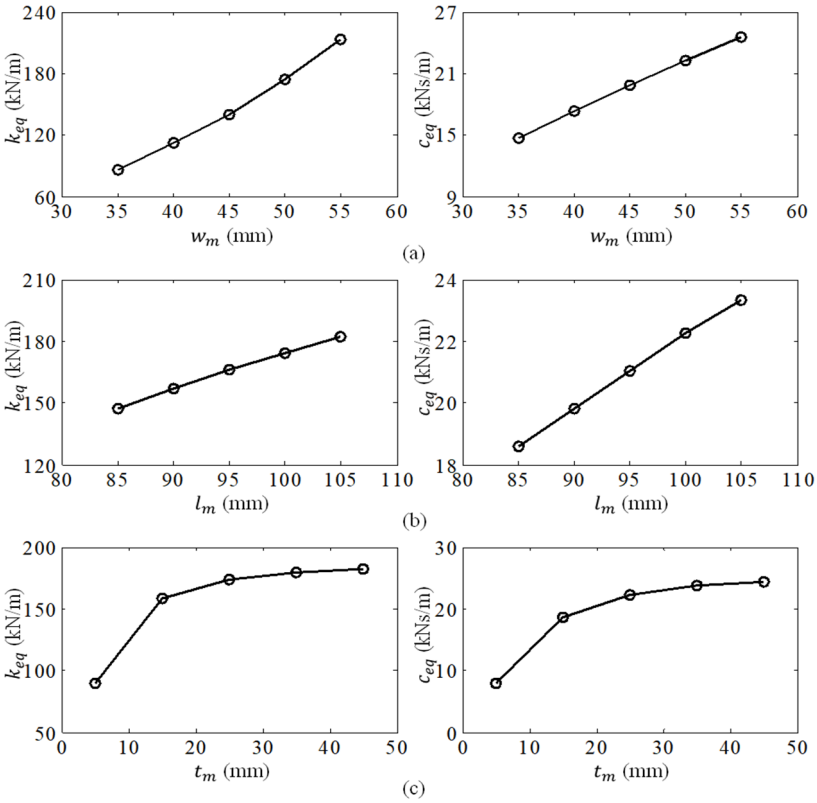


Fig. 11 Variation of the stiffness coefficient $k_{eq}$ and the damping coefficient $c_{eq}$ as a function of (a) width $w_m$; (b) length $l_m$; and (c) thickness $t_m$ of magnet under a harmonic motion with an amplitude $A$ = 10 mm and a frequency $f$ = 5.0 Hz

$\phi$ between eddy-current force and relative velocity mainly contributes to the hysteretic nonlinearity of eddy-current force.

## 4. Effects of different design parameters

The effects of the dimensions of permanent magnets and copper plate, the number of copper-plate layers, and the clear gap on $k_{eq}$ and $c_{eq}$ are explored through parametric case studies of a damping system, under harmonic excitation, simulated in ANSYS (2018).

### *4.1 Dimensions of magnet*

Figs. 11(a)-(c) respectively show the effects of magnet width $w_m$, length $l_m$ and thickness $t_m$ on the equivalent stiffness coefficient $k_{eq}$ and the equivalent damping coefficient $c_{eq}$ of the eddy-current force under a harmonic motion with an amplitude $A$ of 10 mm and a frequency $f$ of 5.0 Hz. Figs. 11(a)-(b) show that both $k_{eq}$ and $c_{eq}$ increase with $w_m$ and $l_m$. The increasing rate of $k_{eq}$ and $c_{eq}$ for $w_m$ and $l_m$ are practically constant. It indicates that the damping capability and the stiffness behavior are enhanced simultaneously by the increase of $w_m$ or $l_m$. It should be noted that the ratio of $k_{eq}/c_{eq}$ is almost constant with $l_m$. As seen from Eqs. (5)-(6), it indicates that the phase lag $\phi$ is insensitive to the variation of magnet length $l_m$, under a given frequency. Fig. 11(c) shows that both $k_{eq}$ and $c_{eq}$ increase with $t_m$, in which the increasing rate decreases with $t_m$. It indicates that increasing the thickness of magnet could improve the damping capability but at the same time enhance the stiffness behavior. The reduction of increasing rate indicates that a magnet with relatively large $t_m$ is not effective for enhancing the damping capability. Overall, this section shows that enlarging the dimensions of magnet simultaneously enhances $k_{eq}$ and $c_{eq}$ due to the increase of magnetic field.

### *4.2 Dimensions of copper plate*

Figs. 12(a)-(c) respectively show the effects of copper-plate width $w_c$, length $l_c$ and thickness $t_c$ on the equivalent stiffness coefficient $k_{eq}$ and the equivalent damping coefficient $c_{eq}$ of the eddy-current force under a harmonic motion with $A$= 10 mm and $f$ = 5.0 Hz. Fig. 12(a) shows that $k_{eq}$ slightly decreases with $w_c$, while $c_{eq}$ slightly increases with $w_c$. The increase of $w_c$ could reduce the existence of stiffness behavior. It could be seen from Eqs. (5)-(6) that the phase lag $\phi$ of the eddy-current force is reduced. From a design point of view, lengthening $w_c$ also increases the allowable movement for the damper. The damper could move with larger amplitude without reducing its damping capability. Fig. 12(b) shows that the variation of $k_{eq}$ and $c_{eq}$ are insensitive the variation of $l_c$. This is because the vibration direction is perpendicular to the length of the copper plate, increasing the length of copper plate would have negligible effects on the dynamic

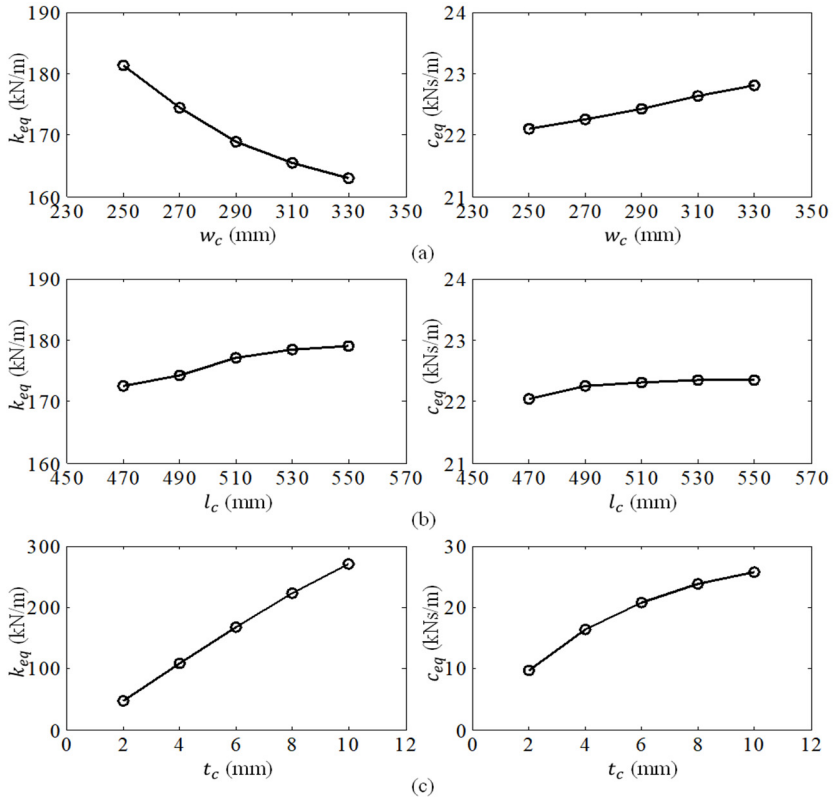


Fig. 12 Variation of the stiffness coefficient $k_{eq}$ and the damping coefficient $c_{eq}$ as a function of (a) width $w_c$; (b) length $l_c$; and (c) thickness $t_c$ of copper plate under a harmonic motion with an amplitude $A$ = 10 mm and a frequency $f$ = 5.0 Hz

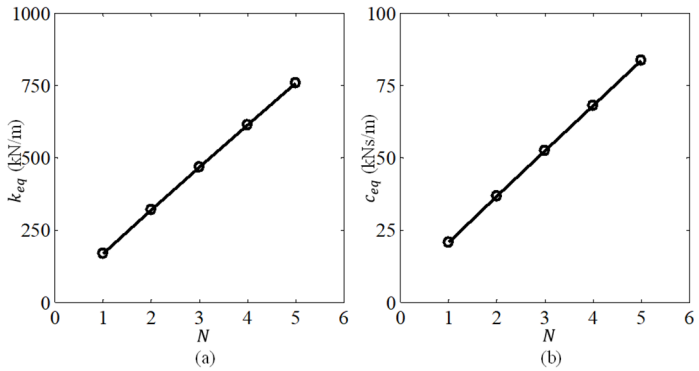


Fig. 13 Variation of the (a) stiffness coefficient $k_{eq}$ and (b) damping coefficient $c_{eq}$ as a function of the number of copper-plate layer $N$ under a harmonic motion with an amplitude $A =$ 10 mm and a frequency $f =$ 5.0 Hz

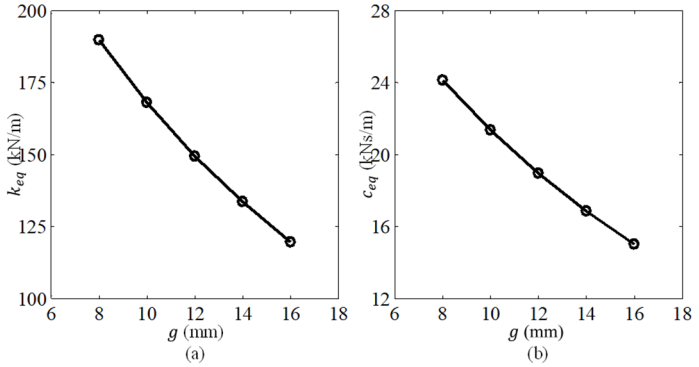


Fig. 14 Variation of the (a) stiffness coefficient $k_{eq}$; and (b) damping coefficient $c_{eq}$ as a function of clear gap $g$ under a harmonic motion with an amplitude $A =$ 10 mm and a frequency $f =$ 5.0 Hz

characteristics of the eddy-current force. It indicates that there is no additional benefit to increase the copper-plate length for enhancing the damping coefficient. The $k_{eq}/c_{eq}$ is also practically constant with $l_c$. It means that the phase lag $\phi$ is insensitive to the length of copper plate $l_c$. Fig. 12(c) shows that both $k_{eq}$ and $c_{eq}$ increase with $t_c$. It indicates that increase of $t_c$ simultaneously enhances the stiffness behavior and the damping capability of the damper. The increasing rate for $k_{eq}$ seems constant while that for $c_{eq}$ slightly decreases with $t_c$. When $t_c$ is comparable to the skin depth (Kazimierczuk 2014), the damping capability is reduced. Hence, the increasing rate of $c_{eq}$ is reduced with $t_c$. Since the increasing rate for $k_{eq}$ to $t_c$ is higher than that for $c_{eq}$ to $t_c$, based on Eqs. (5)-(6), it is shown that the phase lag $\phi$ increases with $t_c$. In other words, the hysteretic nonlinearity of eddy-current force becomes more noticeable when thickness of copper plate increases.

### 4.3 Number of copper-plate layer

Figs. 13(a)-(b) respectively show the effects of the number of copper-plate layer $N$ on the equivalent stiffness coefficient $k_{eq}$ and the equivalent damping coefficient $c_{eq}$ of the eddy-current force under a harmonic motion with an amplitude $A$ of 10 mm and a frequency $f$ of 5.0 Hz. The number of copper-plate layers is defined as the number of copper plates being embedded in between two consecutive rows of magnets. Hence, the number of magnet layer is always equal to the number of copper-plate layers plus one. It can be shown in Fig. 13 that both $k_{eq}$ and $c_{eq}$ are linearly related to the $N$. It indicates the increasing the number of copper-plate layers simultaneously increases the stiffness behavior and the damping capability of the damper. However, it should be noted that the ratio of $k_{eq}/c_{eq}$ of the eddy-current damper with $N = 5$ is quite similar to that with $N = 1$. It indicates that the phase lag $\phi$ is insensitive to the variation of number of copper-plate layers. This finding is useful from a design point of view. During a design stage, when a designer would like to analyze a plate-type eddy-current damper with multiple copper-plate layers, he or she might first examine the eddy-current damper with a single layer of copper plate. This is beneficial as analyzing the eddy-current damper with a single layer requires less computational time for numerical simulation.

### 4.4 Clear gap

Figs. 14(a)-(b) respectively show the effects of clear gap $g$ on the equivalent stiffness coefficient $k_{eq}$ and the equivalent damping coefficient $c_{eq}$ of the eddy-current force under a harmonic motion with an amplitude $A$ of 10 mm and a frequency $f$ of 5.0 Hz. Fig. 14 shows that $k_{eq}$ and $c_{eq}$ decrease with $g$. The reduction is mainly caused by the reduction of the magnetic field experienced by the

copper plate. The equivalent stiffness coefficient $k_{eq}$ and the equivalent damping coefficient $c_{eq}$ are respectively reduced by 37.0% and 37.8% for thickness changed from 8 to 16 mm. Again, similar to the number of copper-plate layers, the ratio of $k_{eq}/c_{eq}$ is almost constant for the range of $g$ considered in the analysis. It indicates that the phase lag $\phi$ is insensitive to the variation of clear gap.

## 5. Application of the proposed Eddy-current Damper on a base-isolated structure

The vibration mitigation performance of the proposed eddy-current damper is examined in this section. The eddy-current damper shown in Fig. 5 is implemented to an idealized linear elastic two-degree-of-freedom base-isolated structure, as shown in Fig. 15. The structure formulated as a shear-beam model is subjected to a harmonic ground motion with an acceleration amplitude of 0.1 m/s$^2$ and an excitation frequency up to 5 Hz. The eddy-current damper under the harmonic motion is modeled as a dashpot element in parallel with a spring element that provide a linear damping force and a linear stiffness force, respectively. Recall that the equivalent damping coefficient $c_{eq}$ and the equivalent stiffness coefficient $k_{eq}$ are sensitive to the variation of vibration frequency, but insensitive to the variation of vibration amplitude (Figs. 9 and 10). Therefore, for each frequency, the equivalent damping coefficient $c_{eq}$ and the equivalent stiffness coefficient $k_{eq}$ of the damper are obtained from Table 2. The dynamic equations describing the base-isolated structure equipped with the eddy-current damper can be written as

$$\boldsymbol{M}\ddot{\boldsymbol{x}} + \boldsymbol{C}\dot{\boldsymbol{x}} + \boldsymbol{K}\boldsymbol{x} = -\boldsymbol{M}\boldsymbol{\Lambda}\ddot{x}_g \tag{7}$$

where $\boldsymbol{x} = [x_b \quad x_s]^T$ is the displacement vector of the structure. $x_b$ and $x_s$ are the relative-to-ground displacement at the base and at the top of the structure, respectively. $\ddot{x}_g$ is the ground acceleration. $\boldsymbol{\Lambda} = [1 \quad 1]^T$ is a vector with entries formed by ones. $\boldsymbol{M}, \boldsymbol{C}, \boldsymbol{K}$ are the mass, damping and stiffness matrices of the structure defined as

$$\boldsymbol{M} = \begin{bmatrix} m_b & 0 \\ 0 & m_s \end{bmatrix}, \quad \boldsymbol{C} = \begin{bmatrix} c_b + c_s + c_{eq} & -c_s \\ -c_s & c_s \end{bmatrix}, \quad \boldsymbol{K} = \begin{bmatrix} k_b + k_s + k_{eq} & -k_s \\ -k_s & k_s \end{bmatrix} \tag{8}$$

where $m_b =$ 12000 kg, $c_b =$ 9.42 kN-s/m, $k_b =$ 1184.4 kN/m are the mass, damping coefficient, and stiffness coefficient at the base of the structure, respectively. $m_s =$ 18000 kg, $c_s =$ 5.65 kN-s/m, and $k_s =$ 4441.3 kN/m are the mass, damping coefficient, and stiffness coefficient at the top of the structure, respectively. Eqs. (7)-(8) are solved numerically using the ordinary differential equation (ode) solver in MATLAB (2018).

Figs. 16(a)-(b) respectively show the base drift amplitude and the absolute acceleration amplitude response spectra at the top of the structure with and without eddy-current damper under the harmonic ground motion. The results for the case of neglecting the nonlinearity of eddy-current force are also presented for comparison. For this case, the damping coefficient of the damper is assumed as $c =$ 24.44 kN-s/m. Results show that the proposed damper reduces the base drift and absolute acceleration when the excitation frequency is closed to the modal frequency of the structure. The proposed damper could reduce the peak of

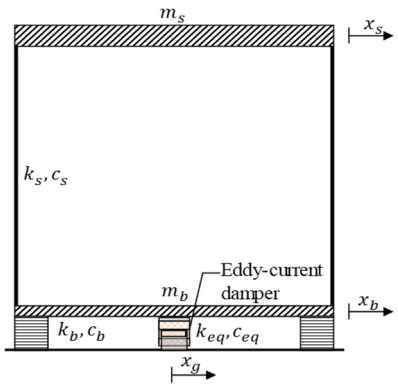


Fig. 15 Implementation of the proposed plate-type eddy-current damper on a base-isolated structure

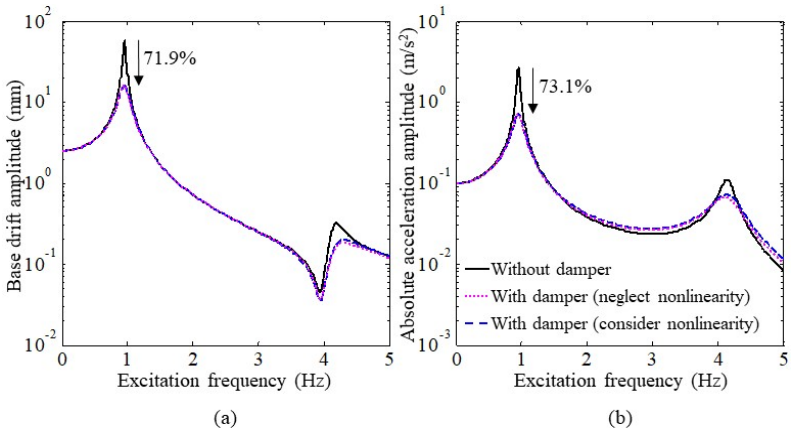


Fig. 16 Response spectra of the base-isolated structure equipped with the proposed eddy-current damper under harmonic ground motion: (a) base drift amplitude; (b) absolute acceleration amplitude

the relative displacement and absolute acceleration response spectra by 71.9% and 73.1%, respectively. Fig. 16 also shows that when the nonlinearity of eddy-current force is neglected, the base drift and absolute acceleration amplitudes of the structure are underestimated. This phenomenon is obvious for a relatively large excitation frequency (see the results of excitation frequency larger than 4.0 Hz). These results indicate that it should consider the nonlinearity of eddy-current force in the analysis in order to obtain a more accurate response estimation.

## 6. Conclusions

This study designs a plate-type eddy-current damper with a high energy-dissipation capability. The proposed damper having a dimension of as 270 mm × 500 mm × 80 mm is made by sixteen pairs of magnets and a copper plate. The magnets are arranged as two rows of 4-by-4 arrays with polarities alternating to the adjacent magnets along the direction of motion. The copper plate is embedded in between the two rows of magnets. A finite-element model is developed to investigate the eddy-current force generated by the damper. Under a constant velocity of 0.2 m/s, the damping coefficient provided by the eddy-current damper is 24.44 kN-s/m, which results in a damping density of 2.26 MNs/m/m$^3$. The eddy-current force is found to have a hysteretic relationship with the relative velocity between the magnet components and the copper plate. The eddy-current force is fitted as the sum of a linear elastic force and a linear damping force that can be characterized with an equivalent stiffness coefficient and an equivalent damping coefficient, respectively. Results show that the stiffness coefficient is increased by about 77 times while the damping coefficient is relatively reduced by about 19% for vibration frequency increased from 0.5 to 10.0 Hz. The variation of the damping and stiffness coefficients on the width, length, and thickness of magnet and copper plate, as well as the number of copper-plate layers together with the clear gap are further analyzed. It is found that the phase lag caused by the hysteretic nonlinearity can be reduced with the increase of copper-plate width, as well as the decrease of copper-plate thickness and magnet width. On the other hand, the phase lag is found to be insensitive to the length of magnet, the length of copper plate, the number of copper-plate layers, and the clear gap. The implementation of the proposed eddy-current damper on a base-isolated structure is further presented. Results show that the proposed damper could reduce the peak of the base drift and the peak of absolute acceleration response spectra by 71.9% and 73.1%, respectively. It should be noted that this study focuses on numerical simulation only. Experimental studies should be conducted in the future to verify the results.

## Acknowledgments

This study is sponsored by the National Science Foundation of China (Grant No: 51878483), and the Key Laboratory of Performance Evolution and Control for Engineering Structures (Tongji University), Ministry of Education (No. 2019KF-6). The third author would like to thank the financial support from the Hong Kong PhD Fellowship Scheme (HKPFS) provided by the Research Grants Council of the HKSAR.

## References

ANSYS (2018), ANSYS Maxwell 3D, ANSYS Electronic 19.0, ANSYS, Inc.

Ao, W.K. and Reynolds, P. (2019), "Evaluation of eddy current damper for vibration control of a frame structure", *J. Physics Commun.*, **3**(5), 055013. https://doi.org/10.1088/2399-6528/ab1deb

Bae, J., Hwang, J., Park, J. and Kwag, D. (2009), "Modeling and experiments on eddy current damping caused by a permanent magnet in a conductive tube", *J. Mech. Sci. Technol.*, **23**(11), 3024-3035. https://doi.org/10.1007/s12206-009-0819-0

Bae, J., Hwang, J., Kwag, D., Park, J. and Inman, D.J. (2014), "Vibration suppression of a large beam structure using tuned mass damper and eddy current damping", *Shock Vib.*, 2014, 893914. https://doi.org/10.1155/2014/893914

Bourquin, F., Caruso, G., Peigney, M. and Siegert, D. (2014), "Magnetically tuned mass dampers for optimal vibration damping of large structures", *Smart Mater. Struct.*, **23**(8), 085009. https://doi.org/10.1088/0964-1726/23/8/085009

Chen, W., Jiang, J., Liu, J., Bai, S. and Chen, W. (2013), "A passive eddy current damper for vibration suppression of a force sensor", *J. Phys. D: Appl. Phys.*, **46**(7), 075001. https://doi.org/10.1088/0022-3727/46/7/075001

Diez-Jimenez, E., Rizzo, R., Gómez-Garcia, M.J. and Corral-Abad, E. (2019), "Review of passive electromagnetic devices for vibration damping and isolation", *Shock Vib.*, **2019**, 1250707. https://doi.org/10.1155/2019/1250707

Ebrahimi, B., Khamesee, M.B. and Golnaraghi, M.F. (2008), "Design and modeling of a magnetic shock absorber based on eddy current damping effect", *J. Sound Vib.*, **315**(4-5), 875-889. https://doi.org/10.1016/j.jsv.2008.02.022

Ebrahimi, B., Khamesee, M.B. and Golnaraghi, M.F. (2009), "Eddy current damper feasibility in automobile suspension: modeling, simulation and testing", *Smart Mater. Struct.*, **18**(1), 015017. https://doi.org/10.1088/0964-1726/18/1/015017

Engineering ToolBox (2001), [Online] Available at: https://www.engineeringtoolbox.com (Last accessed on March 10, 2020).

Feudo, S.L., Allani, A., Cumunel, G., Argoul, P., Maceri, F. and Bruno, D. (2017), "Experimental analysis of a tuned mass damper with eddy current damping effect", Models, Simulation, and Experimental Issues in Structural Mechanics, Springer Series in Solid and Structural Mechanics, Springer, Cham, **8**: 235-248. https://doi.org/10.1007/978-3-319-48884-4_13

Heald, M.A. (1988), "Magnetic braking: improved theory", *Am. J. Phys.*, **56**(6), 521-522. https://doi.org/10.1119/1.15570

Huang, Z.W., Hua, X.G., Chen, Z.Q. and Niu, H.W. (2018), "Modeling, testing, and validation of an eddy current damper for structural vibration control", *J. Aerosp. Eng.*, **31**(5), 04018063. https://doi.org/10.1061/(ASCE)AS.1943-5525.0000891

Kazimierczuk, M. (2014), *High-Frequency Magnetic Components*, (2nd Edition), John Wiley & Sons, Ltd.

Li, J., Zhu, S. and Shen, J. (2019), "Enhance the damping density of eddy-current and electromagnetic dampers", *Smart Struct. Syst., Int. J.*, **24**(1), 15-26. https://doi.org/10.12989/sss.2019.24.1.015

Loong, C.N., Shan, J., Shi, Z. and Chang, C.C. (2020), "Approximate analysis of eddy-current force under time-varying velocity motion for structural control", *J. Sound Vib.*,

**475**, 115295. https://doi.org/10.1016/j.jsv.2020.115295
Lu, X., Zhang, Q., Weng, D., Zhou, Z., Wang, S., Mahin, S.A., Ding, S. and Qian, F. (2017), "Improving performance of a super tall building using a new eddy-current tuned mass damper", *Struct. Control Health Monitor.*, **24**(3), e1882. https://doi.org/10.1002/stc.1882
Lu, X., Zhang, Q., Wu, W. and Shan, J. (2019), "Data-driven two-level performance evaluation of eddy-current tuned mass damper for building structures using shaking table and field testing", *Comput.-Aided Civil Infrastruct. Eng.*, **34**(1), 38-57. https://doi.org/10.1111/mice.12373
MATLAB (2018), 9.7.0.1190202 (R2019b), Natick, Massachusetts: The MathWorks Inc.
Pan, Q., He, T., Xiao, D. and Liu, X. (2016), "Design and damping analysis of a new eddy current damper for aerospace applications", *Latin Am. J. Solids Struct.*, **13**(11), 1997-2011. https://doi.org/10.1590/1679-78252272
Schieber, D. (1975), "Optimal dimensions of rectangular electromagnet for braking purposes", *IEEE Transact. Magnet.*, **11**(3), 948-952. https://doi.org/10.1109/TMAG.1975.1058768
Shi, Z., Shan, J., Wu, W. and Loong, C.N. (2020), "Mechanical modeling of eddy current damping regarding frequency-dependence with test validation". [Under review]
Sodano, H.A., Bae, J., Inman, D.J. and Belvin, W.K. (2005), "Concept and model of eddy current damper for vibration suppression of a beam", *J. Sound Vib.*, **288**(4-5), 1177-1196. https://doi.org/10.1016/j.jsv.2005.01.016
Wang, Z., Chen, Z. and Wang, J. (2012), "Feasibility study of a large-scale tuned mass damper with eddy current damping mechanism", *Earthq. Eng. Eng. Vib.*, **11**(3), 391-401. https://doi.org/10.1007/s11803-012-0129-x
Wang, W., Dalton, D., Hua, X., Wang, X., Chen, Z. and Song, G. (2017), "Experimental study on vibration control of a submerged pipeline model by eddy current tuned mass damper", *Appl. Sci.*, **7**(10), 987. https://doi.org/10.3390/app7100987
Wu, W., Shan, J. and Ruan, K. (2018), "A kind of self-sensing eddy-current type energy consumption replaceable coupling beam", National Intellectual Property Administration, PRC Patent CN207436305U, September 21, 2018.
Zhu, S., Shen, W. and Xu, Y. (2012), "Linear electromagnetic devices for vibration damping and energy harvesting: modeling and testing", *Eng. Struct.*, **34**, 198-212. https://doi.org/10.1016/j.engstruct.2011.09.024
Zuo, L., Chen, W. and Nayfeh, S. (2011), "Design and analysis of a new type of electromagnetic damper with increased energy density", *J. Vib. Acoust.*, **133**(4), 041006. https://doi.org/10.1115/1.4003407

*BS*